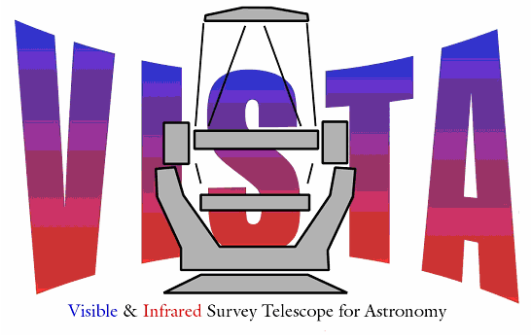

IR CAMERA

Document Title: VISTA IR Detector Characterisation Procedure

Document Number: VIS-PRO-ATC-06032-0003

Issue: Issue 1.1

Date: 29 January 2004

Document Prepared By:	**Naidu Bezawada Electronics Engineer**	**Signature and Date:**	
Document Approved By:	**Mel Strachan ATC Project Manager**	**Signature and Date:**	
Document Reviewed By:	**Gavin Dalton IR Camera Project Scientist**	**Signature And Date:**	
Document Reviewed By:	**Martin Caldwell IR Camera Systems Engineer**	**Signature and Date:**	
Document Released By:	**Kim Ward IR Camera Project Manager**	**Signatures and Date:**	

Change Record

Issue	Date	Section(s) Affected	Description of Change/Change Request Reference/Remarks
Draft 0.1	10-09-03	All	New document
Draft 0.2	20-10-03	1.2	A change in the document number
Issue 1.0	20-10-03		
Issue 1.1	29-01-04	4.8 Appendix-1(new) Appendix-2 (new)	Symbols changed, filter profile inside integral. Radiometric uncertainty. Appendix-1 and 2 added with filter modelling and photon rate derivation

TABLE OF CONTENTS

CHANGE RECORD **2**

1 INTRODUCTION **5**

1.1 PURPOSE 5
1.2 APPLICABLE DOCUMENTS 5
1.3 REFERENCE DOCUMENTS 5
1.4 ABBREVIATIONS AND ACRONYMS 5

2 DEFINITIONS **6**

2.1 UNCORRELATED FRAME 6
2.2 CORRELATED DOUBLE SAMPLED (CDS) FRAME 6
2.3 MINIMUM DETECTOR INTEGRATION TIME 6
2.4 ROW RESET (RIPPLE RESET) 6
2.5 GLOBAL RESET 6
2.6 TEMPORAL NOISE 6
2.7 PIXEL TO PIXEL READ NOISE 6

3 THE TEST SETUP **7**

3.1 DETECTOR MOUNT 7
3.2 FILTER WHEEL 8
3.3 PRE-AMPLIFIER PCB 8
3.4 CONNECTORS AND WIRING 9
3.5 RADIATION SHIELD 9
3.6 FILTERS 10
3.7 CRYOSTAT WINDOW 12
3.8 BLACKBODY 12

4 TESTS **12**

4.1 DETECTOR SENSITIVITY AND SYSTEM GAIN 13
4.1.1 Photon Transfer Technique 13
4.1.2 Histogram based measurement 13
4.1.3 Uncertainty of the measurement 14
4.2 FULL WELL CAPACITY 14
4.3 READ NOISE 14
4.3.1 Pixel to pixel read noise measurement: 14
4.3.2 Temporal noise: 15
4.4 LINEARITY 15
4.5 DARK GENERATION 15
4.5.1 Reset Effect 15
4.6 READOUT GLOW 15
4.7 PERSISTENCE AND CROSS-TALK 16
4.7.1 Persistence 16
4.7.2 Inter Readout Cross-talk 16
4.8 QUANTUM EFFICIENCY MEASUREMENTS 16
4.8.1 Absolute QE 16
4.8.2 Measure at two different temperatures 18
4.8.3 Measure at various blackbody temperatures 19
4.8.4 Relative QE 19
4.8.5 QE at different temperatures 19
4.8.6 Radiometric Uncertainty 19
4.9 DETECTOR DC OUTPUT 20

4.9.1 DC Drift 20
4.10 PIXEL OPERABILITY AND DEFECT MAPS 20
4.10.1 Pixel Connectivity 20
4.10.2 Dark defects map 21
4.10.3 QE defect map 21
4.10.4 Operability map 21
5 TEST REPORT 21
APPENDIX-1 22
APPENDIX -2 25

1 INTRODUCTION

VPO has contracted RVS to produce IR detectors for VISTA IR camera. The RVS will supply 16 IR science detectors that fully meet specifications laid in [AD1], 4 engineering grade detectors and 3 bare multiplexers as per [AD2]. RVS has delivered 3 bare multiplexers in October 2002. A test facility has been set up at ATC with primary responsibility to characterise the IR detectors as they are delivered.

1.1 Purpose

This document presents the details of the test facility and the test procedures that will be carried out on the VISTA IR Detectors (VIRGO 2k x 2k) at ATC. The document presents the sequence of test procedures and the format of the results that will be produced in due course.

1.2 Applicable documents

[AD1] IR Detector technical specification, VIS-SPE-ATC-06020-0003, Issue 3.0, 13 June 2002

[AD2] IR Detectors statement of work, VIS-SOW-ATC-06020-0002, Issue 2.0, 13 June 2002

1.3 Reference documents

[RD1] VIRGO Pre-amplifier Design and Performance, VIS-TRE-ATC-06032-0006, Issue 1.0, 13 November 2003

[RD2] Text book: Fundamentals of infrared detector operation and testing, John David Vincent, Wiley Series on Pure and Applied optics 1990

[RD3] Radiometry MathCAD program, Peter Love, Raytheon Vision systems

[RD4] MathCAD Program, David Lee, ATC

1.4 Abbreviations and acronyms

ADC	Analog to Digital Converter
ADU	ADC digital Unit
ATC	UK Astronomy Technology Centre
CDS	Correlated Double Sample
DN	Digital Number (same as ADU)
IR	Infrared
IRACE	InfraRed Array Controller Electronics
VPO	VISTA Project Office
VIRGO	A 2k x 2k HgCdTe (2.5µm cut-off) IR detector

VISTA	Visible Infrared Survey Telescope for Astronomy
RVS	Raytheon Vision Systems

2 Definitions

2.1 Uncorrelated frame

The array is reset, allowed to integrate and readout.

2.2 Correlated double sampled (CDS) frame

The array is reset and then a first readout is performed. Charge is allowed to integrate for a desired integration time after which a second readout is performed. The first readout frame is subtracted from the second read frame digitally pixel-by-pixel to obtain a CDS frame.

2.3 Minimum detector integration time

The detector minimum integration time is equal to time taken to perform a single readout of the array.

2.4 Row reset (Ripple reset)

The array is reset row-by-row. A row is reset after it has been read or accessed before advancing to next row.

2.5 Global reset

All the pixels in the detector are reset simultaneously or held under reset continuously and released from reset at same time meaning that all the pixels start integrating charge at same time.

2.6 Temporal noise

Noise estimated from a set of CDS frames taken sequentially with minimum possible time interval between individual frames. A noise (standard deviation) frame is constructed from the noise measured pixel-by-pixel from all CDS frames. The mean of the noise histogram is the temporal read noise.

2.7 Pixel to pixel read noise

Pixel to pixel read noise is measured from two CDS dark frames with minimum detector integration time. The two frames are subtracted from each other. The standard deviation estimated from of a region free of defects in the resulted frame divided by √2 is the pixel to pixel read noise in a CDS frame.

3 The test setup

All the VIRGO detectors will be characterised using the test facility at ATC as described below. The test facility comprises a cryostat with a closed cycle cooler and IRACE controller. The low background test cryostat includes a detector mount suitable for VIRGO detector, a manually operated cold filter wheel in front of the detector and a pre amplifier fan-out board close to the detector.

3.1 Detector mount

The detector mount contains a temperature controlled stage which can be operated from 50K to 90K. The temperature of the detector mount stage is regulated to ±0.01K from the set temperature using a Lakeshore temperature controller (model 331). The detector mount is electrically isolated from the rest of the cryostat using sapphire spacers to allow a separate ground control for the detector mount. The minimum temperature that the detector mount can reach is 45K. The detector is surrounded by a low background baffle on the detector mount to prevent scattered light reaching the detector. The bottom section of the cryostat in figure 1 shows the detector mount stage, pre-amplifier fan-out PCB and pillars for filter wheel mount.

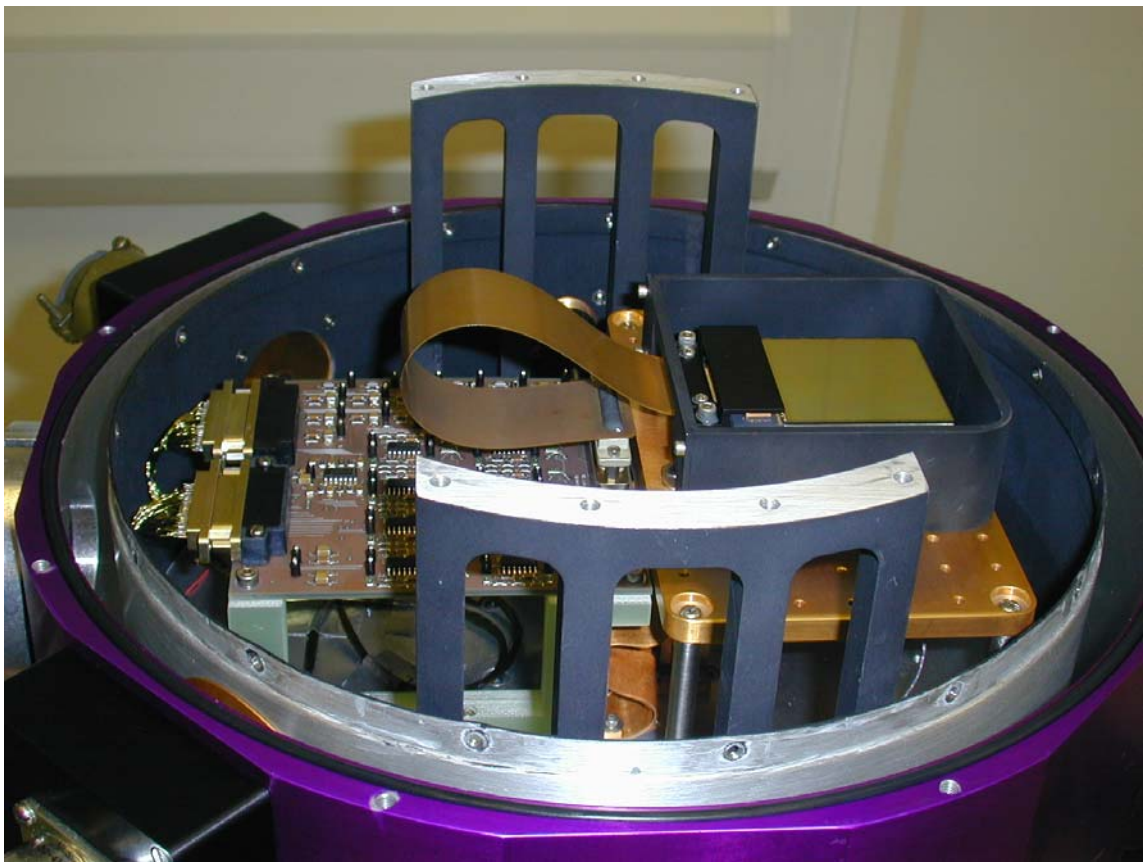

Figure 1: Detector mount in the test cryostat (A Virgo multiplexer is shown in picture)

3.2 *Filter wheel*

The cryostat is integrated with a filter wheel that holds J, H, K filters and a blank. Figure 2 shows the filter wheel housing mounted above the detector mount. The filter wheel is operated manually through a vacuum feed through and filter position is indicated by indicator knob outside the cryostat. The filter wheel allows the detector to be illuminated through J, H and K filters for quantum efficiency, uniformity measurements and mapping of defect / hot pixels. A cold blank is positioned in front of the detector for estimating dark current generation and image persistence tests. Above the filter wheel housing is a cold baffle tube shielding the scattered light from the light path. The baffle tube can also hold cold aperture place holders at adjustable heights. A cold aperture of 1.5mm size is installed inside the baffle tube at a known height from the detector plane to define 'f#' for estimating the photon flux at the detector plane.

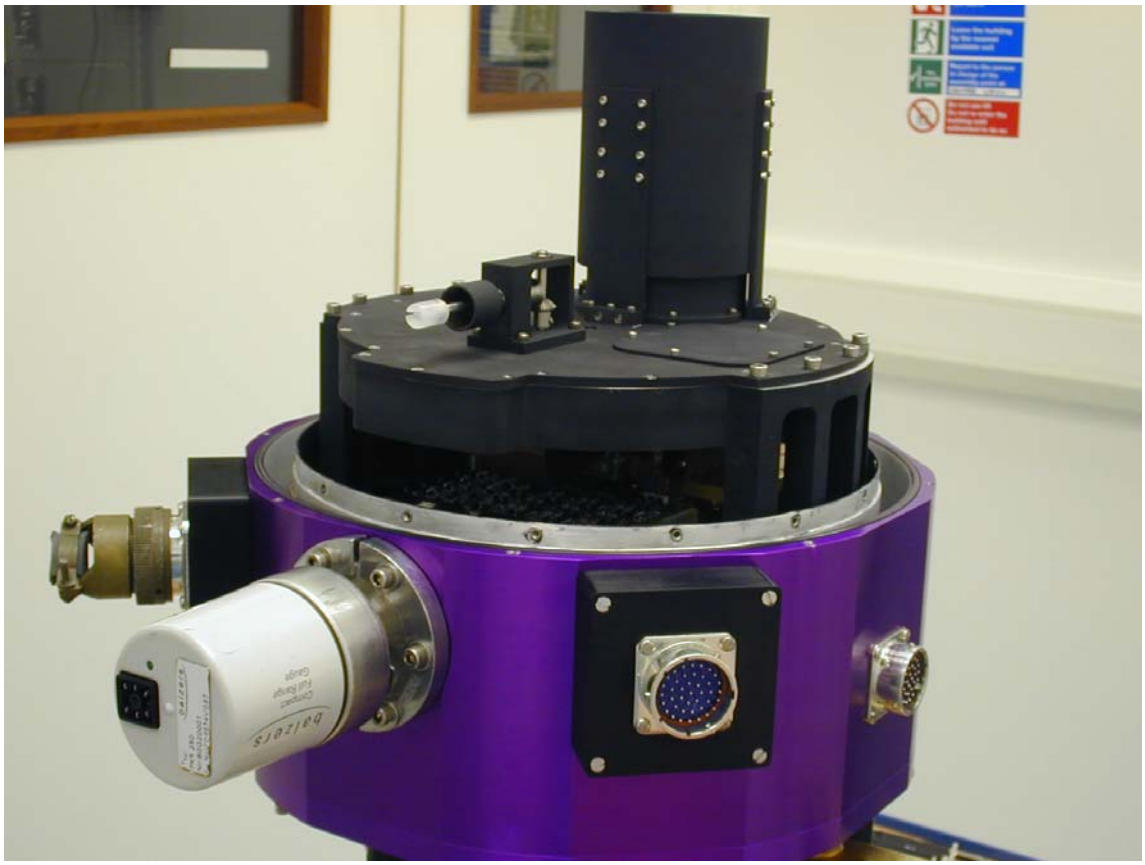

Figure 2: Filter wheel housing in the test cryostat

3.3 *Pre-amplifier PCB*

Close to the detector mount located is a 16-channel differential pre-amplifier fan-out board. The differential pre-amplifiers use TLC2274 CMOS op-amps which work reliably at temperatures well below (approximately down to 45K) detector operating temperature (72K). The schematic of the pre-amp configuration is shown in figure 3. The pre-amplifier gain is set

at 4.78. The output signal from detector is modulated on a DC level of about 3.1V. This DC offset is removed using a reference voltage generated from the IRACE controller. The differential outputs of each pre-amp are DC coupled to the acquisition modules of IRACE. The bias and clock voltages from IRACE are further filtered and over-voltage protected with clamping zener diodes in the pre-amp board. Details of the design are available in RD1.

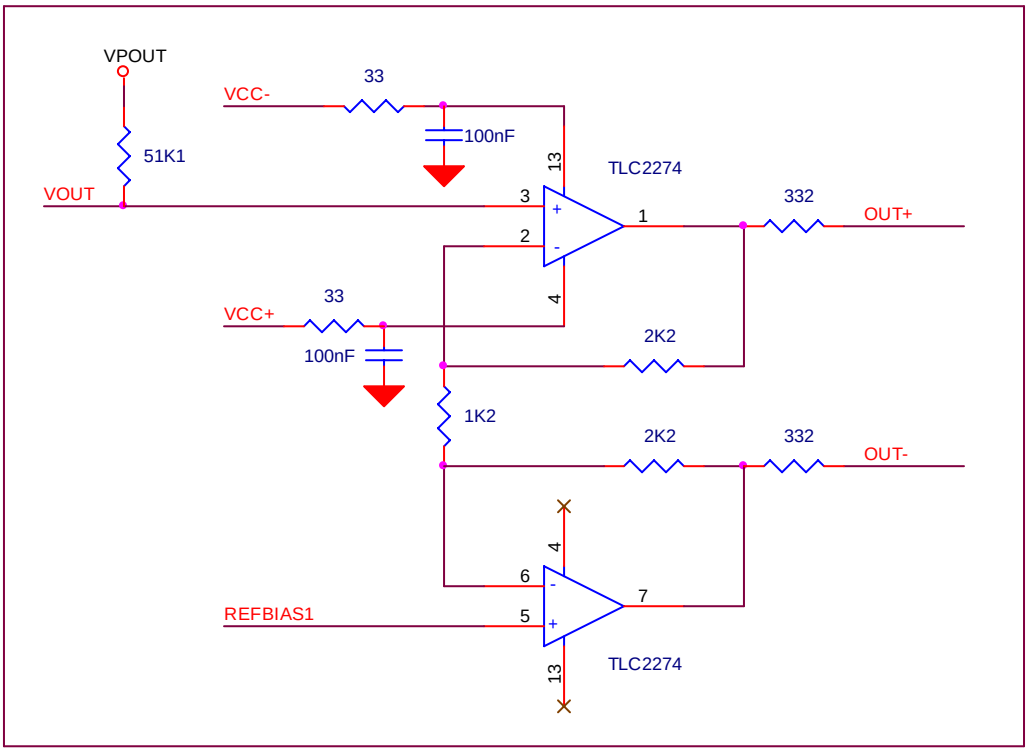

Figure 3: Schematic of pre-amplifier configuration (Shown for single channel)

3.4 *Connectors and wiring*

The cryostat contains three hermetic connectors, two of which (55-pin and 41-pin) are used to separate the bias, clock voltages and signal outputs from each other. The other hermetic connector is used for temperature sensors and heater connections. The wiring harness goes through heat sinks attached to the radiation shield in order to reduce the background radiation. A standard evacuation port (KF-40) with valve to pump out and a port for a pressure gauge to monitor the vacuum level are provided. The external wiring includes a screened cable for biases, a screened cable for clocks and another screened cable for signal outputs between the cryostat and the detector controller.

3.5 *Radiation shield*

The detector mount and the filter wheel assembly are surrounded by a low background radiation shield (top radiation shield). The top radiation shield is attached to a radiation shield in the bottom section of the cryostat (bottom radiation shield) which is mounted directly on to

the cold plate. The cold plate temperature is around 42K during operation. Figure 4 shows the assembled top radiation shield and a small baffle around the entrance aperture on top radiation shield cover.

Figure 4: Assembled radiation shield surrounding detector mount & filter wheel (left) and a cover on the top radiation shield with supports (right)

3.6 Filters

The filters have been procured from NDC. These filters are processed along with WFCAM science filters with same specifications. These are 58mm x 58mm, 5mm thick in size. The transmissions of the filters are measured by the manufacturer both at warm and cold (120K) temperatures. The slope of the edge shift with temperature (the cut-on and cut-off) from warm to cold is linearly extrapolated to the filter temperature 45K. The cut-on and cut-off values (50% points) for all the three filters are shown in the table 1. Figures 5, 6 and 7 show the transmission characteristics of the J, H and K filters respectively.

Table1: Filter data

Filters	293K		120K		45K (extrapolated)		Transmittance (% avg.)
	Cut-on (µm)	Cut-off (µm)	Cut-on (µm)	Cut-off (µm)	Cut-off (µm)	Cut-on (µm)	
J-Band	1.189	1.354	1.184	1.348	1.350	1.181	84.05
H-Band	1.495	1.782	1.481	1.769	1.773	1.474	87.47
K-Band	2.120	2.448	2.100	2.410	2.425	2.060	79.32

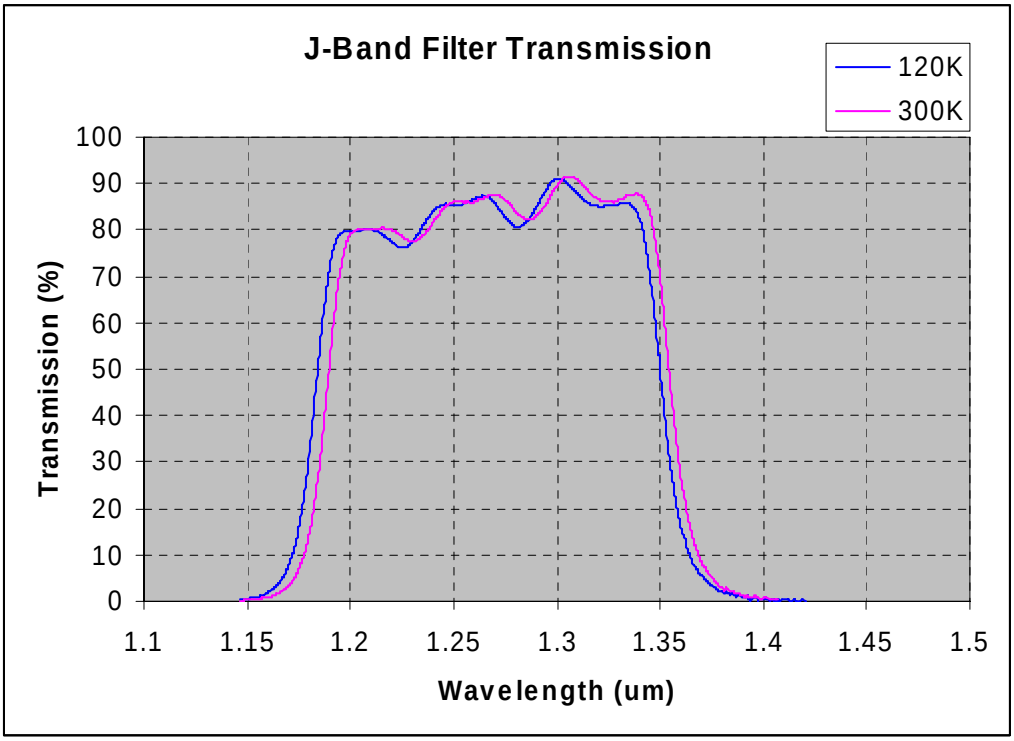

Figure 5: J-Band filter transmission curves

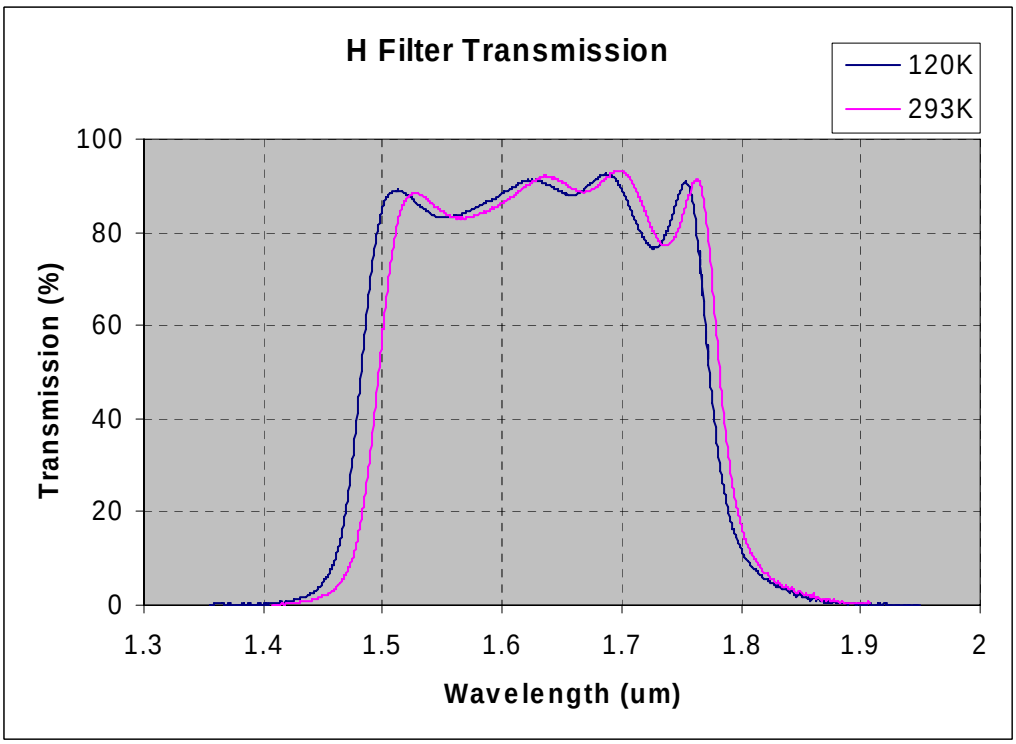

Figure 6: H-Band filter transmission curves

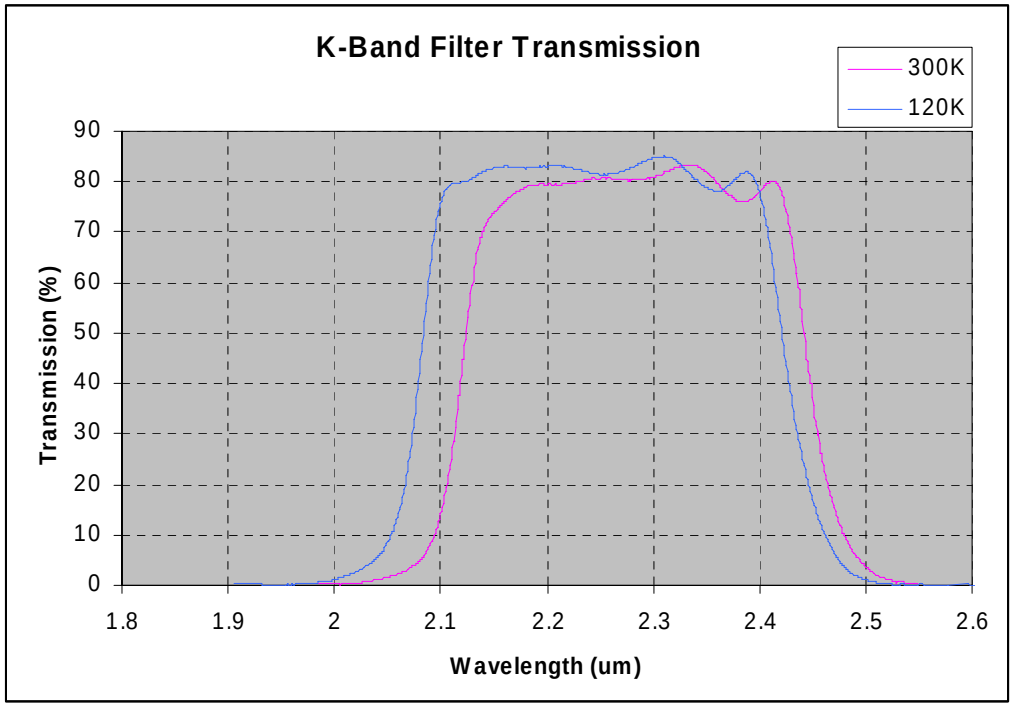

Figure 7: K-Band filter transmission curves

3.7 Cryostat window

The cryostat window is a 64mm diameter clear aperture CaF2 window. There are no antireflection coatings on the window and transmission is 0.95.

3.8 Blackbody

An extended area blackbody (4"x4", model 4004 from SBIR) is used to illuminate the detector and for QE measurements. The operating temperature range of the blackbody is 50 - 600ºC, settable to 0.1ºC resolution using the blackbody temperature controller (model 930 from SBIR). The emissivity of the source is 0.93 (±0.03).

4 Tests

The detector is operated at 280 KHz pixel rate in each channel, with 16 output channels allowing a frame readout time of 1 sec. A row-by-row reset is used for resetting the detector. The following performance tests will be performed on every detector.

- Signal gain and noise
- Dark generation
- Well depth and linearity
- Quantum efficiency
- Operability and mapping of defects

Persistence and cross-talk measurements will be done on one or two detectors.

4.1 Detector Sensitivity and System Gain

The system gain relates the output digital numbers (DN or ADU) to the corresponding input electrons collected at the pixel unit cell. The system gain is expressed in units of electrons / ADU. With the knowledge of system gain and gain in the signal processing chain (pre-amp gain), the detector internal conversion gain (in units of µV / electron) can be determined. System gain is determined using photon transfer technique.

4.1.1 Photon Transfer Technique

Photon transfer technique gives an accurate estimate of the system gain determined through several sets of flats acquired with the system. The system gain is found by measuring the noise as a function of the input flux at high signal levels where shot noise dominates the readout noise. The gain is derived from a plot of noise versus mean signal after pixel to pixel non-uniformity has been removed (flat-fielded).

The experimental method involves collecting several pairs of flat images with counts (ADU) ranging from above the bias level (a dark frame with minimum detector integration time) to near saturation by varying exposure times. The noise is calculated for a small region (e.g. 40 x 40 pixels) free from pixel defects after pixel to pixel non-uniformity has been removed. The pixel non-uniformity is removed by subtracting the two similar flats obtained with same exposures under identical conditions. The noise in the difference flat is divided by √2 to account for the subtraction. The mean signal is obtained from the same region using both frames. The noise and the mean signal data is obtained from several such small regions in the frame. Similarly, the noise and the mean data points are obtained at various signal level from all the pairs of the flat images. A transfer plot is generated on a log-log scale (mean signal on X-axis and noise on Y-axis). The shot noise dominated part of the curve is characterised by a line slope of ½. The intercept of this ½ slope line on signal axis gives the system gain in units of electrons per ADU.

The detector internal conversion gain can be found by:
Conversion gain ($\mu V/e^-$) = (System Gain (e^-/ADU) * A * ADC_{CONV})$^{-1}$
where, A is the preamplifier gain, and ADC_{CONV} is the transfer function of ADC in ADU/µV.

4.1.2 Histogram based measurement

The system gain is also estimated from a gain histogram using the following equation:
System gain = Signal (ADU) / (Signal noise (ADU)^2 – Read noise (ADU)^2)

The read noise in the above equation is estimated from two similar dark frames (with minimum detector integration). The two dark frames are subtracted one from another and the resultant frame is divided by √2. Read noise (in ADU) is the standard deviation of the resultant noise frame from defect free regions.
The gain is estimated from a number of small regions within the array and a histogram of the gain data is plotted. The mean of the gain histogram is the system gain in e/ADU. The gain data points significantly away from the mean of the histogram are eliminated in estimating the mean as they are probably caused by the defect pixels.

4.1.3 Uncertainty of the measurement

The uncertainty in the above gain measurement depends on the number of pixels in a sub-region from which each gain data point is estimated. The uncertainty is estimated from the following equation:
Total gain uncertainty (e/ ADU) = √(2/No.of Pixels) * Mean of Gain histogram

4.2 Full well capacity

The full well capacity (or charge handling capacity) is estimated from the photon transfer plot. The noise (or variance) increases linearly with the input signal (flux). Once the signal level approaching the full well capacity, a noise roll-over is reached due to pixel saturation effects where noise no longer obeys Poisson's statistics.

Since the full well capacity is dependent on the applied detector bias, the detector bias is varied until the required detector full well capacity is obtained. As altering the detector bias slightly alters the detector pixel capacitance and so the system gain. So, for every detector bias the system gain is measured.
The detector bias is given by:
Detector bias = Pixel reset voltage (VrstUc) – Detector common voltage (VdetCom)

The detector bias is thus varied by either VrstUc or VdetCom. The higher VrstUc gives higher DC output level which is not desired due to the input common mode voltage limitations at the IRACE acquisition modules. Hence the VDetCom is varied in order to have the minimum possible DC level at the output to achieve the desired detector bias. All the further tests are carried out at this detector bias level.

4.3 Read noise

4.3.1 Pixel to pixel read noise measurement:

Two CDS dark frames each with minimum detector integration time are subtracted from each other pixel-by-pixel. The standard deviation estimated from a defect free region of the resultant frame is divided by √2 and multiplied by the system gain to get the pixel to pixel read noise in electrons rms. This noise is referred as read noise in a CDS frame.

4.3.2 Temporal noise:

Series of CDS dark frames are obtained with minimum detector integration time without any time interval between individual frames. A noise frame (in ADU) is generated by measuring noise in every pixel from all the dark frames on pixel-by-pixel basis. The resultant noise frame is converted into electrons by multiplying with the system gain. A histogram of the noise frame in electrons is generated. The mean of the histogram is the temporal read noise. The standard deviation of the histogram shows the noise uniformity.

4.4 Linearity

The data frames obtained for estimating the system gain are used to plot the mean output signal vs. integration time. The output signal in ADU is converted into electrons multiplying with the system gain. A least square fit is fitted to the data from 10% to 80% of the full well. The non-linearity is obtained from the following equation:

Non-linearity (%) = ((Measured data / Fit data) – 1) * 100

A non-linearity plot is generated with the signal values on X-axis and corresponding non-linearity on Y-axis. The non-linearity (peak to valley) is estimated from the plot.

4.5 Dark generation

Series of dark frames are obtained each with 100s integration time and an average dark frame is generated. The frame is then converted from into electrons/sec and a histogram is generated. The mean of the histogram shows the average dark in e/s and the sigma of the histogram gives the uniformity of the dark generation. A gray scale map of the average dark frame is presented. Dark generation tests will be carried out at 65K, 72K, 77K and 82K operating temperature.

4.5.1 Reset Effect

The dark generation versus the time after reset plot is generated to see if the resetting has any effect on the dark generation (for example immediately after reset). A set of non destructive dark frames at equal intervals following the resetting are obtained. Mean dark generation frames at the sampled time are obtained by subtracting the first frame from the second frame, second frame from the third frame and so on. A plot with the mean signal (in electrons) on Y-axis versus the time of sample on X-axis is generated. The mean dark signal close to the reset deviates from linearity if there is a reset effect on the dark generation.

4.6 Readout glow

The additional dark generation due to resetting or reading the array is estimated by taking series of non-destructive dark frames at equal intervals and from a simple CDS dark frame of equivalent integration time (time taken to obtain N non-destructive samples). A multi-sampled CDS frame is generated by subtracting the first frame in the N frames from the N^{th} frame. The simple CDS frame is subtracted from the multi-sampled CDS frame. The resultant frame is converted into electrons by multiplying with the system gain. The resultant frame is

then converted into a glow per readout frame by dividing with no of non-destructive readouts. Histogram and gray scale plots of the glow frame will be presented.

4.7 Persistence and cross-talk

4.7.1 Persistence

A small portion of the detector (few tens of pixels) is exposed to the input flux such that the exposed pixels saturate in about second. Collimated blackbody radiation through a small cold aperture is considered. The input flux is doubled (by increasing the blackbody temperature) to allow the exposed pixels hard saturated. Soon after the saturation the cold blank is positioned before the detector and a sequence of CDS frames are acquired. The CDS frames are investigated for the persistence signal decay till a minute after pixel saturation.

4.7.2 Inter Readout Cross-talk

A CDS frame is acquired with pixels (preferably belonging to any one of the 16 readout channels) exposed to close to saturation. The CDS frame is examined for shadows or ghost images of the exposed pixels in all other readout channels in the frame. If there is electrical cross-talk among the readout channels, enhancement in the intensity in corresponding pixels processed through other readout channels become apparent.

4.8 Quantum efficiency measurements

4.8.1 Absolute QE

The quantum efficiency of the detector will be measured in J, H and K pass bands using blackbody radiometry [RD2], [RD3]. The flux incidence on the detector plane at a given blackbody temperature is estimated from the following equations. The transmission characteristics of the filters and the window are also used for these measurements. The schematic of the QE setup is shown in the figure 8 and the procedure is described below. The QE measurements will be carried out at 65K, 72K, 77K and 82K operating temperature.

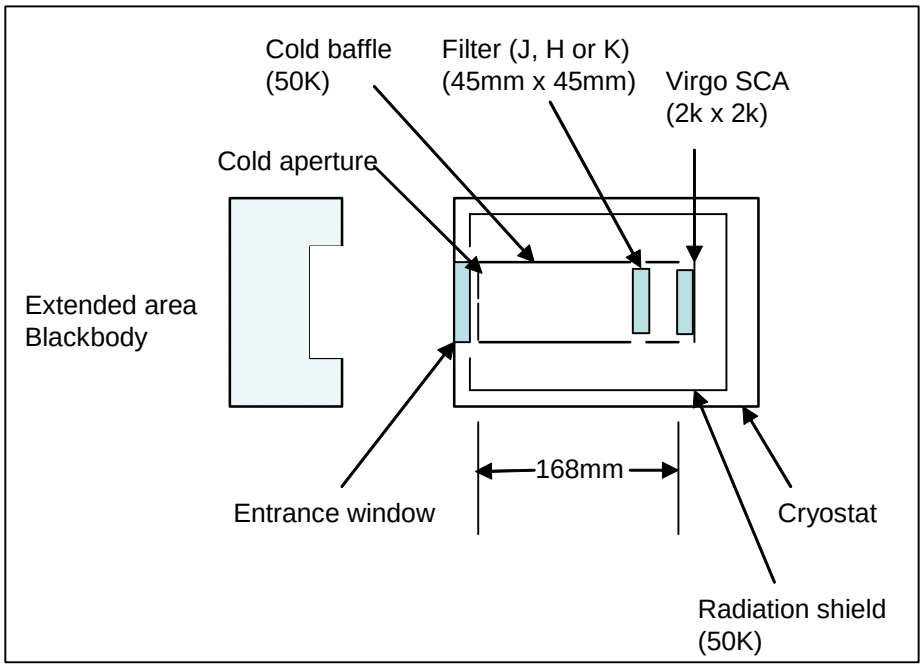

Figure 8: Schematic of the setup

The spectral photon exitance (photons emitted into hemisphere per unit area per second per unit spectral bandwidth) from a blackbody emitting surface is calculated by Planck's law:

$$M_q(\lambda, T_{bb}) := 2\cdot\pi\cdot\frac{c}{\lambda^4}\cdot\frac{\varepsilon}{\left(e^{\frac{h\cdot c}{\lambda\cdot k\cdot T_{bb}}}-1\right)} \quad \text{photons}\cdot\text{cm}^{-2}\cdot\text{s}^{-1}\cdot\mu\text{m}^{-1}$$

h = Planck's constant (6.626276 x 10^{-34} Joule. Sec)
k = Boltzmann constant (1.380662 x 10^{-23} Joule.K^{-1})
c= Speed of light (2.99792458 x 10^{8} m.sec^{-1})
ε = Emissivity of blackbody (0.93)

The in-band photon exitance through the cryostat window with transmission 'T_{window}' and through a band pass filter ($\lambda_{low} < \lambda < \lambda_{high}$) with a transmission '$T_{filter}(\lambda)$' can be calculated by the integral:

$$M\left(T_{bb}\right) := T_{window} \cdot \int_{\lambda_{low}}^{\lambda_{high}} T_{filter}(\lambda) \cdot 2 \cdot \pi \cdot \frac{c}{\lambda^4} \cdot \frac{\varepsilon}{\left(e^{\frac{h \cdot c}{\lambda \cdot k \cdot T_{bb}}} - 1\right)} \, d\lambda$$

λ_{low} = Cut on limit wavelength of the filter
λ_{high} = Cut off limit wavelength of the filter

The filter transmission data measured at room temperature at ATC is transformed to the desired cold temperature (45K) by using a transformation derived from the data provided by NDC (filter manufacturer) on the test filter at both warm (293K) and cold (120K) temperatures [RD4]. The transformation is shown in appendix-1 (for J-band filter).

The circular aperture with diameter D above the detector plane at a distance of H reduces the projected solid angle from that of a hemisphere (π) by a factor of $(D/2H)^2$. The irradiance produced at the detector plane is then given by

$$\text{Irradiance (E)} = M(T_{bb}) * (D/2H)^2 \text{ photons. cm}^{-2}.\text{sec}^{-1}$$

An alternative derivation of the power and photon rate at the detector plane is given in appendix-2 provided by Matt Griffin.

4.8.2 Measure at two different temperatures

The irradiance is estimated at two different blackbody temperatures 'T_{bb_lo}' and 'T_{bb_hi}' using the above integral.

$$\Delta E = M(T_{bb\_hi}) - M(T_{bb\_lo}) \quad \text{photons.cm}^{-2}.\text{sec}^{-1}$$

The effective quantum efficiency is then estimated from

$$QE := \frac{\Delta V}{T_{int} \cdot Z_o \cdot A_{opt} \cdot \Delta E}$$

ΔV = Difference in signal output obtained from the detector in volts.
Z_o = Conversion gain of the detector output (V/e)
A_{opt} = Pixel area (4.0×10^{-6} cm^2)
T_{int} = Integration time. (1.001sec)

QE is determined for every pixel in the array and a QE histogram is generated. Gray scale maps and QE histograms for QE in all three bands are generated. The QE non-uniformity is estimated from the sigma and the mean of the histogram.

Uniformity = Sigma / Mean

4.8.3 Measure at various blackbody temperatures

QE is also estimated from the CDS frames with same integration time obtained at various blackbody temperatures. Input flux on the detector plane is estimated at every blackbody temperature as described above. A plot with the signal (in Volts) from detector versus the estimated photon flux (photons/cm^2/integration time) is generated. The signal level varies linearly with the input flux. Quantum efficiency is determined from the slope of the plot using the following relation.

QE = Slope / (Conversion gain in V/e * Pixel area in cm^2)

The intercept of the fit shows any systematic errors in estimation. If there are no systematic errors, the intercept should be close to zero.

4.8.4 Relative QE

The relative spectral response from 0.8µm to 2.7µm can be measured by using a monochromator at desired wavelengths. The throughput of the monochromator / integrating sphere can be calibrated by a NIST calibrated sensor / radiometer. As an example either pyroelectric or thermopile detectors whose spectral response is flat can be used. The sharpness of the cut-off and cut-on can be determined from the relative response. The experimental setup for this is under consideration.

4.8.5 QE at different temperatures

The detector QE and uniformity will also be determined at 60K, 70K and 80K operating temperature. Detector cosmetics and uniformity tend to improve at lower temperatures while absolute QE tends to reduce at lower operating temperatures.

4.8.6 Radiometric Uncertainty

The uncertainties in the radiometry are dominated by the uncertainties in the temperature of the blackbody, emissivity of the blackbody and spectral band-pass transmission. The actual uncertainties may be bigger due to unwanted reflections and light scattering within the test cryostat. The uncertainty values are estimated for the test cryostat from equations in RD2.

Table 2: Radiometric uncertainty in the test cryostat

Parameter	Value	Uncertainty	Contribution
Emissivity	0.93	0.03	3.2%
Aperture diameter(mm)	1.0mm	0.010mm	2.0%
Aperture distance(mm)	163	1	1.2%
J-band			
Temperature(K)	600	2	6.3%
Wavelength(µm)	1.265	0.005	5.9%
Bandwidth(µm)	0.17	0.005	2.9%
Total (RSS)			9.9%
H-band			
Temperature(K)	500	2	7.1%
Wavelength(µm)	1.623	0.005	4.2%
Bandwidth(µm)	0.299	0.005	1.7%
Total (RSS)			9.3%
K-band			
Temperature(K)	400	2	8.0%
Wavelength(µm)	2.242	0.005	2.7%
Bandwidth(µm)	0.365	0.005	1.4%
Total(RSS)			9.4%

The uncertainty in the estimation of transimpedance conversion is around 7%. Combining this with the radiometry uncertainty, the total uncertainty in QE measurements is around 12 to 13% in the present setup.

4.9 Detector DC output

4.9.1 DC Drift

Uncorrelated frames with minimum detector integration are obtained while operating the detector at different temperatures (from 60K to 80K). The data is converted into voltage at the detector output. The detector output voltage (V) on Y-axis is plotted with the operating temperature (K) on X-axis. The slope of the plot gives the detector output drift with temperature (V/K). The drift is then converted into equivalent electrons per degree Kelvin by dividing the slope with the conversion gain (V/e).

4.10 Pixel operability and defect maps

4.10.1 Pixel Connectivity

Two uncorrelated frames are obtained corresponding to VdetCom at 0.5V and 0.6V. The two frames are subtracted frame from each other. The histogram of the resultant frame is generated. The DC shift of the pixels connected through indium-bumps will be around 0.1V.

A map of pixels whose DC level has not been shifted is generated and these are the pixels that have indium bumps open.

4.10.2 Dark defects map

The data used to estimate the dark generation is used generate a map of pixels whose dark is greater than 8e/s and less than 0.1e/s (or suitable lower limit). The pixels that showed opens in the pixel connectivity test should also be present in the dark pixel map as they generate no dark current.

4.10.3 QE defect map

From the QE frames in each band, a map of pixels whose QE is <50% of the mean QE of the frame and less than the minimum QE requirement is generated. A combined QE defect pixel map is generated from the QE pixel maps in J, H and K bands.

4.10.4 Operability map

The pixel connectivity map, dark defects map and QE pixel defects map are combined to produce final pixel operability map. This map will be used to estimate the total operability. The pixel connectivity test will be performed after every thermal cycle of the detector in order to identify any new pixels become inoperable following a thermal cycle. The pixel operability map can also be generated at three different operating temperatures (60K, 70K and 80K) to see the detector cosmetic performance.

5 Test Report

The test report with all the above test results will be accompanied with the detector applied biases voltages, measured currents, clock voltages, and timing sequence (pixel frequency) and operating temperature of the detector.

---oOo---

Appendix-1

Filter transmission modelling

NDC provided the edge shift with temperature measurements on a sample filter.

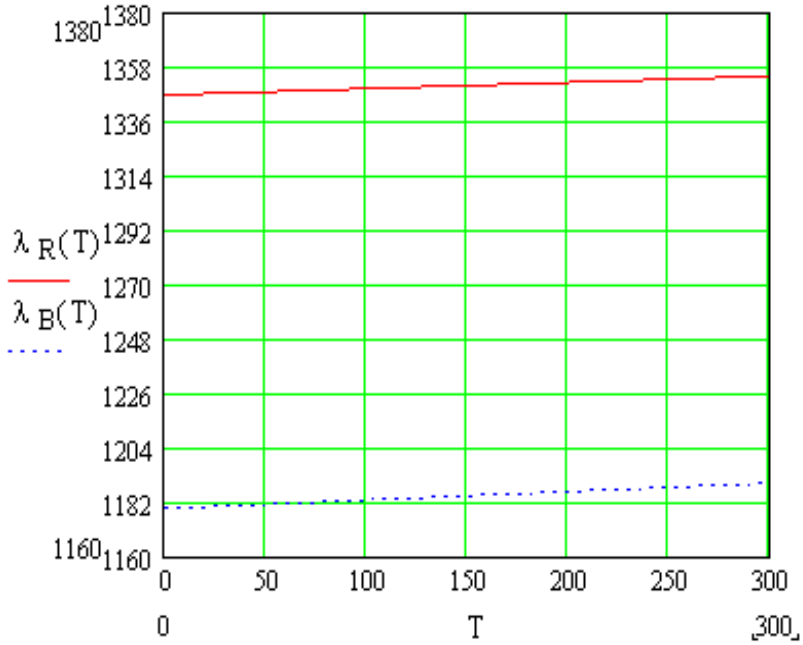

The data on the sample filter is linearly extrapolated to the desired temperature. The red line for room temperature, blue line at 120K and black line at desired temperature (45K).

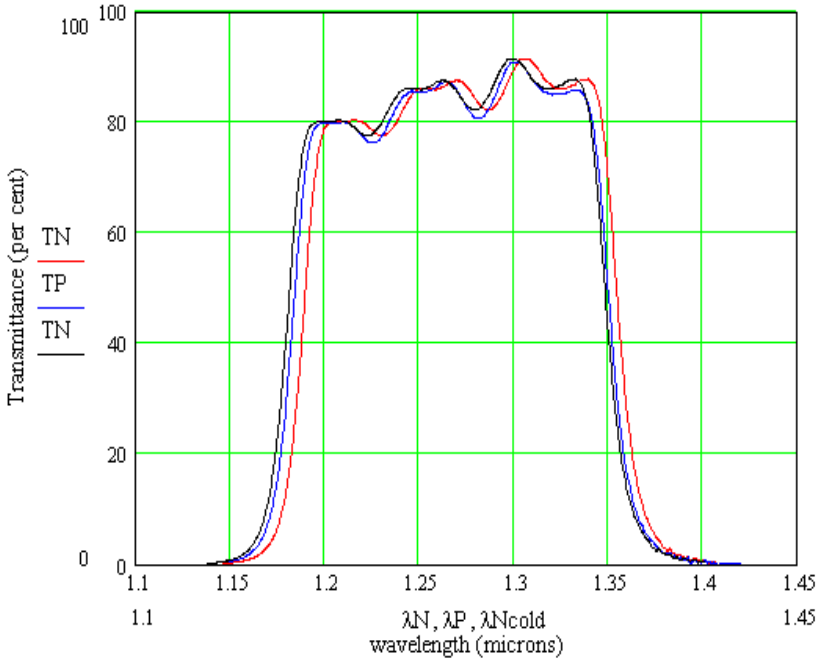

The measured data on the actual filter is then transformed to the desired temperature. The red line is at room temperature and blue line is at required temperature.

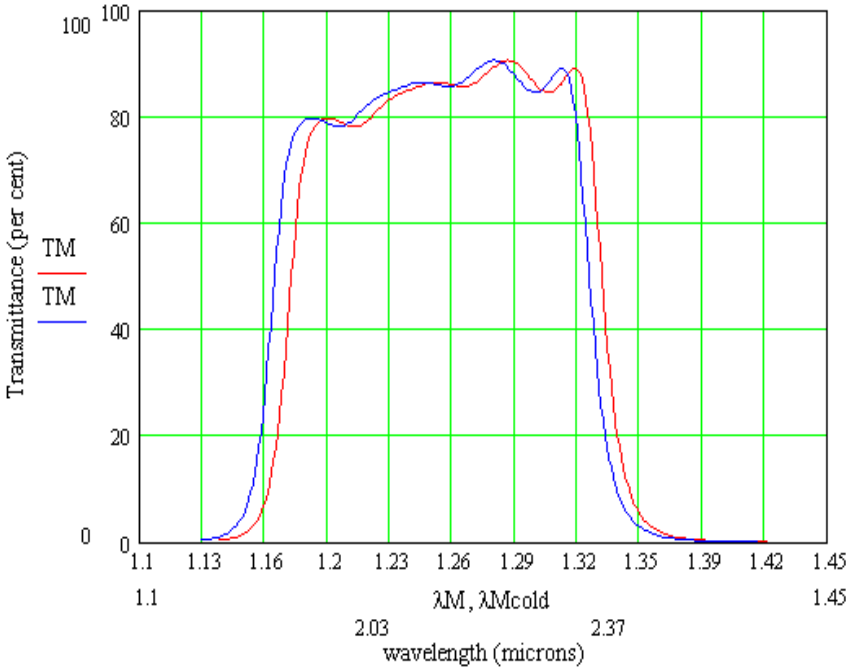

The transformed data is then fit with a cubic spline function.

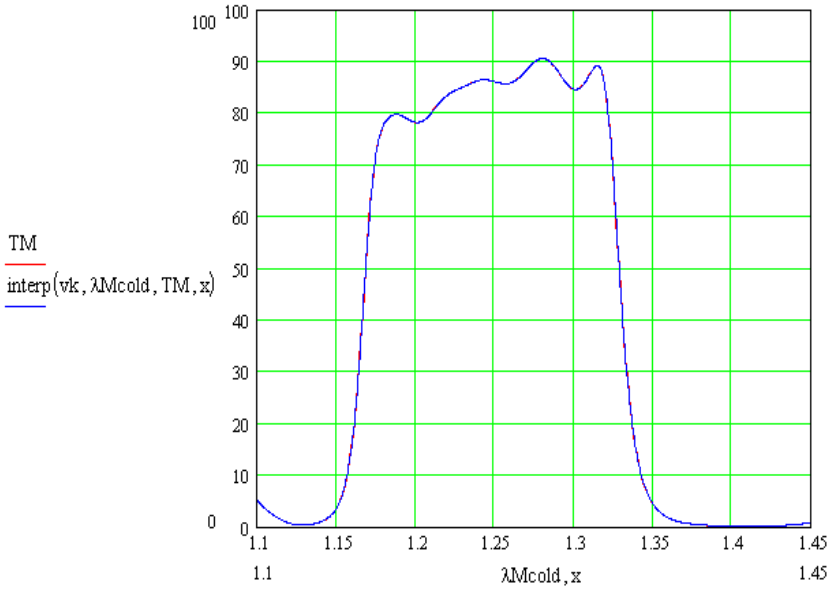

$$M(Tbb) := Twindow \cdot \int_{\lambda low}^{\lambda high} \frac{interp\left(vk, \lambda Mcold, TM, \frac{\lambda}{\mu m}\right)}{100} \cdot 2 \cdot \pi \cdot \frac{c}{\lambda^4} \cdot \frac{\varepsilon}{\left(e^{\frac{h \cdot c}{\lambda \cdot k \cdot Tbb}} - 1\right)} \, d\lambda$$

The filter profile is now taken inside the integral.

Appendix -2

Derivation of power and photon rate for VISTA IR detector calibration facility

The specific intensity (spectral radiance) radiated by black body (power emitted per unit projected area per unit solid angle per unit spectral bandwidth) is

$$B_\lambda(T) = \frac{2hc^2}{\lambda^5 (e^{hc/\lambda kT} - 1)} \qquad \text{W m}^{-2}\ \text{sr}^{-1}\ \text{m}^{-1}$$

The corresponding photon rate is

$$N_\lambda(T) = \frac{2c}{\lambda^4 (e^{hc/\lambda kT} - 1)} \qquad \text{photons s}^{-1}\ \text{m}^{-2}\ \text{sr}^{-1}\ \text{m}^{-1}$$

The total power emitted per unit area per unit spectral bandwidth (radiant excitance) is

$$Q(\lambda,T) = \int B_\lambda(T)\cos\theta d\Omega = B_\lambda(T)\int_0^\infty \cos\theta 2\pi\theta \mathrm{d}\theta = \pi B_\lambda(T) \qquad \text{W m}^{-2}\ \text{m}^{-1}$$

This power is radiated anisotropically into 2π sr: the power emitted by a patch of unit area at an angle θ to its normal is $B_\lambda(T)\cos\theta$. But the illumination of a detector which views the black body face-on through a small solid angle is dictated only by the intensity radiated along its line of sight, $B_\lambda(T)$.

The solid angle subtended by black body aperture at detector is π(half-angle)^2:

$$\Omega = \pi\left[\frac{D}{2H}\right]^2 \text{ sr}$$

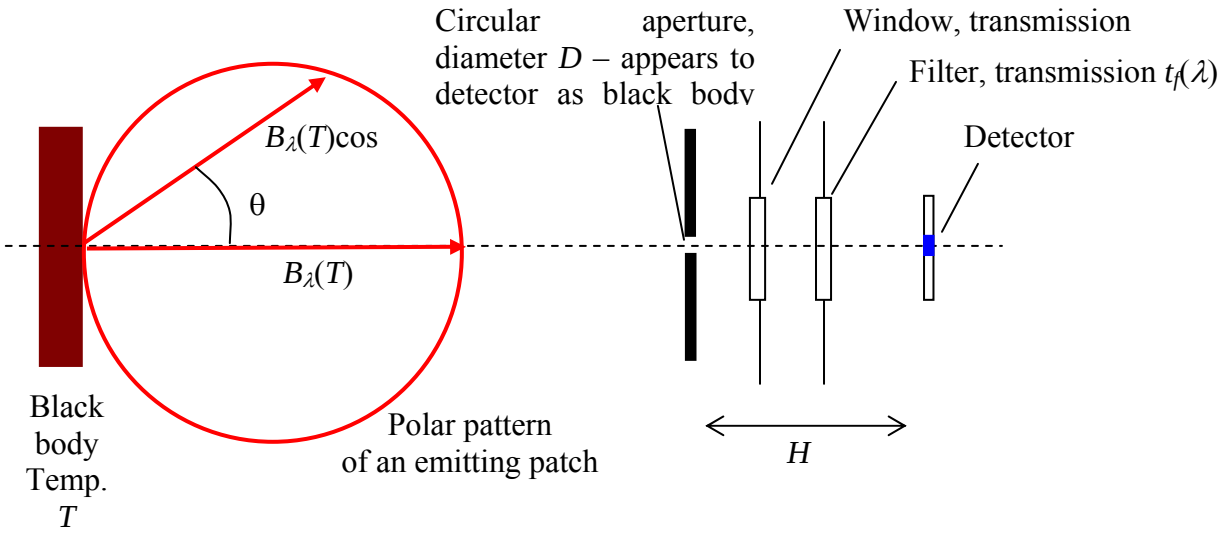

The power per unit area incident on the detector is

$$Pd_{\lambda}(T) = \Omega \int_0^{\infty} t_w(\lambda) t_f(\lambda) B_{\lambda}(T) \mathrm{d}\lambda \ \ \mathrm{W\ m^{-2}}\ .$$

The corresponding incident photon rate is

$$Nd_{\lambda}(T) = \Omega \int_0^{\infty} t_w(\lambda) t_f(\lambda) N_{\lambda}(T) \mathrm{d}\lambda \ \ \mathrm{Photons\ s^{-1}\ m^{-2}}$$

So

$$Nd_{\lambda}(T) = \left[\frac{D}{2H}\right]^2 \int_0^{\infty} t_w(\lambda) t_f(\lambda) \frac{2\pi c}{\lambda^4 (e^{hc/\lambda kT} - 1)} \mathrm{d}\lambda\ .$$

This is equivalent to the equation for irradiance (p.18 + bottom p. 17) in the *Detector Characterisation Procedure* document.